Dalton Transactions

RSC Publishing

PAPER

Metal complexes with functionalised 2,2'-dipicolylamine ligand containing an antioxidant 2,6-di-*tert*-butylphenol moiety: synthesis and biological studies†

Cite this: *Dalton Trans.*, 2013, **42**, 6817

Elena R. Milaeva,*[a,b] Dmitry B. Shpakovsky,[a] Yulia A. Gracheva,[a] Sophia I. Orlova,[a] Viktoryia V. Maduar,[a] Boris N. Tarasevich,[a] Natalia N. Meleshonkova,[a] Ludmila G. Dubova[b] and Elena F. Shevtsova[b]

Received 16th January 2013,
Accepted 19th February 2013

DOI: 10.1039/c3dt50160d

www.rsc.org/dalton

A series of Zn, Mn, Fe, Co, and Ni complexes ([MX_2**L**], X = Cl, OAc) of the novel di-(2-picolyl)amine ligand **L** with an antioxidant 2,6-di-*tert*-butylphenol pendant were synthesized and characterized by elemental analysis, IR, multinuclear NMR spectroscopy, MALDI-TOF mass spectrometry and the molecular structures of [$ZnCl_2$**L**] and [$MnCl_2$**L**] were established by X-ray crystallography. The chemical oxidation of complexes with a 2,6-di-*tert*-butylphenol fragment to the phenoxyl radicals was studied by means of ESR method. The antioxidant radical scavenging activity of the complexes was measured spectrophotometrically using a DPPH-test and linoleic acid peroxidation. The electron transfer reactions were examined in CUPRAC tests and as the inhibition of an enzymatic reaction involving the generation of a reactive oxygen species (superoxide radical-anion) by xanthine oxidase. The lipoxygenase (LOX) inhibition activity of the studied compounds was evaluated. The *in vitro* biological experiments were performed by using rat brain homogenates. The role of the phenol fragment and metal was found to be essential in antioxidant activity.

Introduction

The design of metal-based pharmaceuticals depends on either the ligand scaffold or the choice of metal ion and its oxidation state.[1–3] Polydentate ligands containing 2-pyridylmethyl fragments attached to a nitrogen atom contain both s-donor and p-acceptor binding sites.[4–6] The dipicolylamine (DPA) as a ligand was first reported in 1964.[7] This ligand is known to form stable complexes with numerous metal cations. Zn–DPA complexes are popular for molecular recognition.[8] The three nitrogens of DPA can coordinate strongly to a Zn^{2+} cation, with an association constant in water around 10^7 M^{-1}, leaving one or perhaps two vacant coordination sites for an anionic guest. Furthermore, it is straightforward to incorporate multiple DPA units into a single organic scaffold. One of the first examples of fluorescent chemosensors consisting of a zinc–dipicolylamine appended anthracene derivative can efficiently bind and sense adenosine triphosphate.[9] Later, the fluorophore-linked zinc complexes were used as sensors for phosphatidylserine-containing membranes.[10] Iron(II) and cobalt(II) complexes containing polydentate DPA ligands and their derivatives have been the subject of considerable interest due to their use as model systems for biologically important molecules.[11,12]

Metal complexes of a sterically hindered *N*,*N*,*O* bis-(2-picolyl)(2-hydroxy-3,5-di-*tert*-butylbenzyl)amine were synthesized as models of several hydrolytic enzymes.[6,13,14] The latest investigations of Cu(II) complexes with ethyl 2-[bis(2-pyridylmethyl)amino]propionate interaction with DNA have demonstrated the cytotoxicity.[15]

On the other hand, metal complexes containing antioxidative 2,6-di-*tert*-butylphenol groups have shown activity as antioxidants, inflammatory agents, and scavengers for reactive oxygen species, which makes them promising agents in complex therapy.[16–19] The approach based on the modification of phenolic antioxidants *via* the incorporation of metal in their molecules seems to be a promising one. Previously, for the series of metalloporphyrins with 2,6-di-*tert*-butylphenol groups we demonstrated that the antioxidative activity depends dramatically on the nature of metal ion.[20,21]

Metal complexes containing 2,6-di-*tert*-butylphenol ligands are also of interest because they might provide a synergetic antioxidant effect, acting both as essential organic radical

[a]*Department of Chemistry, Lomonosov Moscow State University, Lenin Hill 1-3, Moscow, 119991, Russian Federation. E-mail: milaeva@org.chem.msu.ru*
[b]*Institute of Physiologically Active Compounds of Russian Academy of Sciences, Chernogolovka, Moscow Region, 142432, Russian Federation*

†CCDC 888418 and 888419. For crystallographic data in CIF or other electronic format see DOI: 10.1039/c3dt50160d

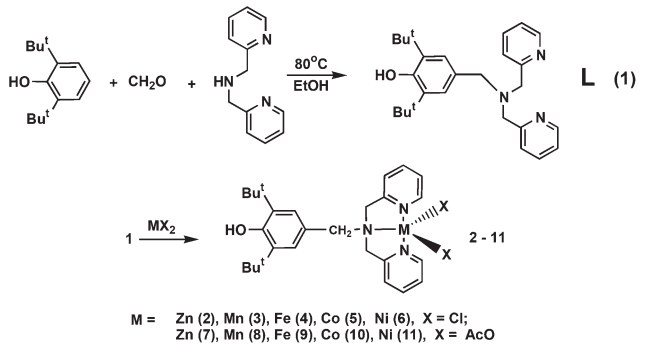

Scheme 1

scavengers and redox-active agents due to the presence of the metal binding site.[22]

Herein, we report the synthesis, structures, redox properties and *in vitro* antioxidant effects of a series of new Zn, Mn, Fe, Co, and Ni complexes containing the [*N*-(3,5-di-*tert*-butyl-4-hydroxybenzyl)-*N*,*N*-di-(2-pyridylmethyl)]amine ligand (**L** or **1**) (Scheme 1). The metal complexes **2–11** could be described as polytopic agents since their molecules possess both organic antioxidant phenol groups capable of hydrogen atom transferring and a transition metal center that is capable of electron transfer.

The formation and stability of phenoxyl radicals was illustrated by ESR. The biological properties of complexes **2–11** have been studied in model radical reactions (DPPH-test, linoleic acid peroxidation), electron transfer processes (CUPRAC method, generation of superoxide radical-anion in the enzymatic reaction of xanthine–xanthine oxidase). In addition to measuring the antioxidant properties in model reactions, their *in vitro* activities in experiments in the lipid peroxidation process in intact mitochondria and cortex neurons isolated from rat brain correspondingly were also examined.

Results and discussion

Syntheses

Ligand. [*N*-(3,5-Di-*tert*-butyl-4-hydroxybenzyl)-*N*,*N*-di-(2-pyridylmethyl)]amine (**L**, **1**) was first reported in 1981 by Grinstead to apply during metals extraction, although, the synthesis of the compound of interest was not described.[23] In this study, the ligand **L** (**1**) was synthesized in 67% overall yield by aminomethylation reaction of 2,6-di-*tert*-butylphenol by bis[(2-pyridyl)methyl]amine in ethanol under reflux condition. Two series of complexes (chlorides and acetates: [MX_2**L**] (X = Cl, OAc; M = Zn, Mn, Fe, Co, Ni, **2–11**) were readily prepared by mixing the appropriate metal salts and **1** in equimolar ratio in relevant solvents (EtOH, MeOH, Me_2CO, MeCN) at room temperature or under reflux condition (Scheme 1).

Compounds **1–11** are crystalline substances stable in the air and in solutions. The Fe^{2+} complexes **4** and **9** were quite stable, although they were stored under argon atmosphere to prevent possible iron oxidation. The compounds were fully characterised by IR, UV-vis, ^1H and ^{13}C NMR spectroscopy (**2**, **6**), MALDI TOF mass spectrometry, and elemental analysis.

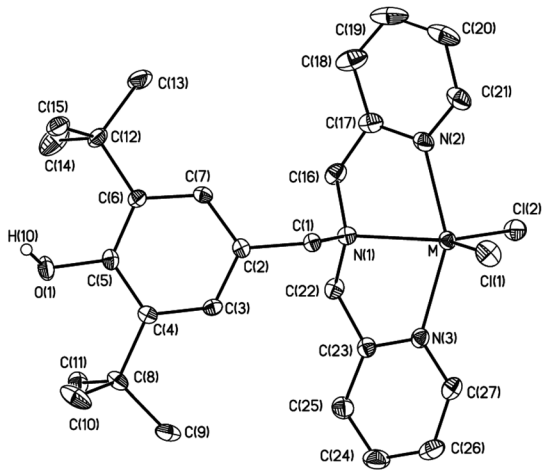

Fig. 1 The general view of **2** [$ZnCl_2$L] and **3** [$MnCl_2$L] in representation of atoms by thermal ellipsoids (p = 50 %). Selected bond lengths (Å): Zn(1)–N(2) 2.1581(14), Zn(1)–N(3) 2.1619(13), Zn(1)–N(1) 2.1955(13), Zn(1)–Cl(2) 2.2658(6), Zn(1)–Cl(1) 2.2712(7), Mn(1)–N(3) 2.2388(11), Mn(1)–N(2) 2.2442(12), Mn(1)–N(1) 2.2809(11), Mn(1)–Cl(2) 2.3559(4), Mn(1)–Cl(1) 2.3722(4).

Crystal structures

The Zn and Mn complexes **2** and **3** crystallized as colorless prisms in a few minutes after the mixing of reagent solutions and they were used for crystallographic analysis. The X-ray diffraction investigation of **2** and **3** has revealed that the complexes are isostructural and crystallize as ethanol solvates. In both complexes, the metal atom is coordinated by two pyridyl nitrogen atoms, one amine nitrogen atom and two chloride ions (Fig. 1). The resulting coordination polyhedron in **2** and **3** can be described as a distorted trigonal bipyramid with N(1), Cl(1) and Cl(2) atoms in the equatorial plane. The N(2)–M–N(3) angle is equal to 151.03(5) and 146.88(4)° in [$ZnCl_2$L] and [$MnCl_2$L], respectively, the conformation of the ligand **L** in the both complexes is almost identical.

Analyzing the crystal packing in **2** and **3** we have found that the hydroxyl group participates in the weak O–H···Cl hydrogen bond (O···Cl is 3.340(1) and 3.340(1) Å in Mn and Zn complexes, respectively) assembling the molecules into centrosymmetric dimers (Fig. 2). Although in the above dimer the two C(2)–C(7) aromatic planes of the adjust molecules are parallel, the smallest C···C separation (C(3)···C(7) is 3.638(3) and 3.610(3) for Zn and Mn complexes, respectively) is too large to expect a significant contribution of the stacking interaction.

Vibrational spectroscopy

The solid IR spectrum of ligand **1** shows strong vibrational bands at 1431, 1592 cm^{-1}, which are assigned to δ vibrations of aromatic system (pyridine and phenol groups), and 2825–2958 cm^{-1} ν(CH). The IR spectra of the above complexes in the 2000–400 cm^{-1} region have mainly a function of fingerprints, the absorption bands being too numerous for a

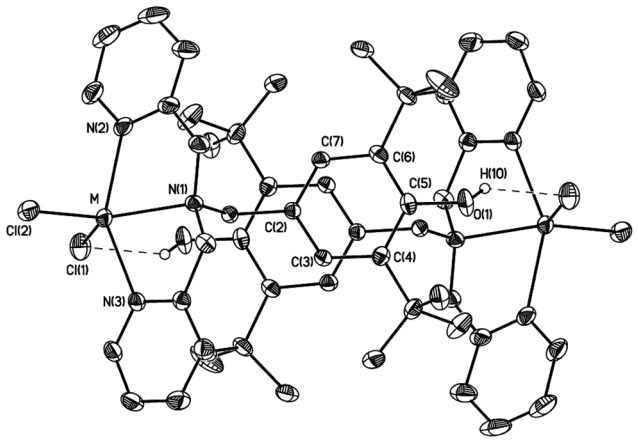

Fig. 2 The general view of centrosymmetric O–H···Cl bonded dimers in **2** [$ZnCl_2L$] and **3** [$MnCl_2L$].

reasonably correct assignment. The broad absorption band is observed in the IR spectrum of **1** in the 3300–3400 cm^{-1} region corresponding to the stretching vibrations of the O–H bond of the hindered phenol associated OH group. After complex formation in the IR spectra of **2–11** the characteristic ν(OH) absorption band of the non-associated phenol group has appeared in the 3600–3680 cm^{-1} region. The shifts of the characteristic ν(OH) absorption bands for complexes **2–11** at 2249–2246 cm^{-1} to a region of higher frequencies when compared with non-coordinated ligands confirm the N-coordination of the ligand and the redistribution of electron density in the di-picolylamine complexes. As it is well known for hindered phenols with donor substituents in the *para*-position in non-coordinating and non-polar solvents the phenol group is not involved in hydrogen bond formation and in the IR spectra the OH stretching are registered in the region of 3600–3650 cm^{-1}.[24] According to elemental analysis data and IR spectra of the Co and Ni acetates **10** and **11**, in which the absorption band of the non-associated phenol group appeared in the 3638–3676 cm^{-1} region and broad bands at 3200–3500 cm^{-1} were found as well, the complexes exist as dimers with one coordinated H_2O molecule.

NMR spectroscopy

Of the complexes, only Zn complexes **2** and **6** are diamagnetic. Similar Mn, Fe, Co and Ni complexes were found to be paramagnetic and gave broad signals as demonstrated by the NMR resonances. The spin S in similar transition metal complexes was estimated to be equal to 1.[25,26]

The characteristic signals of the *tert*-butyl protons and hindered phenol group are shifted in the spectra of the Zn complexes in comparison with those of ligand **1**, confirming the ligand–metal coordination. At room temperature in the ^1H NMR spectrum of chloride **2** the methylene protons attached to pyridyl rings were equivalent and displayed as singlets at 4.14 ppm. In the case of the acetate complex **7** a pair of broadened signals were seen at δ_H 4.18 and 4.28 ppm, which could be doublets from diastereotopic methylene protons. The

Table 1 UV-vis data of the ligand **1** and metal complexes **2–11** (MeOH, 25 °C)

Compound	M	λ_{max} (ε, M^{-1} cm^{-1})
1	—	263 (7296), 268 sh; 283 sh
2	Zn	262.5 (9556); 269.5 sh
7	Zn	231; 256; 262.5 (10 355); 269.5 sh; 281.5 sh
3	Mn	232.5 sh; 257.5 sh; 262.5 (8908); 268.5 sh
8	Mn	232.5 sh; 57.5 sh; 262.5 (8919); 268.5 sh
4	Fe	233 sh; 258 (9401); 281 sh; 385 (1422), 419 sh
9	Fe	262.5 (13 860); 419.5 (1645); 495 (371) sh, 680 sh
5	Co	262.5 (6956); 269 sh; 281.5 sh; 487, 546 (41), 611 sh
10	Co	230 (8232); 262 (6236); 403 (127); 520 (60)
6	Ni	233.5; 256; 261 (7842); 269 sh; 281 sh; 387; 634 (10)
11	Ni	233.5; 256.5; 261 (6810); 268.5 sh; 385, 600 (11)

sh – shoulder.

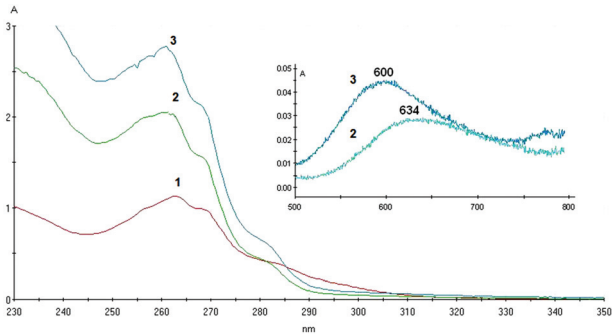

Fig. 3 UV spectra for: ligand **1** 0.155 mM (1); [$NiCl_2L$] **6** 0.265 mM (2); [$Ni(OAc)_2L$] **11** 0.406 mM (3) in CH_3OH. The long wave bands are sketched out in the insertion.

similar phenomenon was observed for the substituted tris(2-pyridylmethyl)-amine Zn complex.[26]

Electronic spectra

The spectral data (λ and ε) of all the complexes and ligand **1** are presented in Table 1. Metal complexes, except those of Zn and Mn, are colored in solid state and in solutions. The electronic absorption spectra of the Ni complexes **6** and **11** are shown in Fig. 3 as examples. Intensive short-wave absorption is arising below 230 nm because of π–π transitions in aromatic systems. The visible bands of the other metal complexes are assigned to d–d transitions and give information about the stereochemistry in solution.

An intensive band is observed in the electron spectra of ligand **1** in the region of 263 nm (see Table 1). This band has a complicated contour due to the superposition of a few bands of electron transitions in the phenolic part of a molecule $^1B_{2u} \leftarrow {}^1A_{1g}$ and allowed on symmetry transition $^1B_1 \leftarrow {}^1A_1$ in pyridine fragments. These bands remain in the spectra of all the complexes, however, the molar absorption coefficient ε changes from 6244 to 13 860 M^{-1} cm^{-1} for different compounds.

In solution, for the spectra of Mn complexes **3** and **8** and Zn complexes **2** and **7**, in addition to absorption at 257–269 nm no long-wave bands were observed. One could

Table 2 Parameters of ESR spectra of phenoxyl radicals **1′–11′** (*a*, G; 290 K)

Radical (M)	Solvent	*g*-factor	a_N	a_{2H} Phenoxyl fragment	a_{2H} Methylene fragment	Number of lines in spectrum
1′	Toluene	2.0030	1.90	1.82	10.9	15
2′ (Zn)	THF	2.0046	2.99	1.80	8.9	13
3′ (Mn)	Toluene/THF	2.0035	—	—	—	[a]
4′ (Fe)	Toluene	2.0046	1.90	1.82	11.0	15
5′ (Co)	Toluene	2.0049	—	1.55	11.0	12
6′ (Ni)	Toluene	2.0046	—	1.62	11.2	12
7′ (Zn)	Toluene	2.0047	1.90	1.82	11.1	15
8′ (Mn)	Toluene	2.0047	1.90	1.82	11.1	15
9′ (Fe)	Toluene	2.0045	1.89	1.80	11.0	15
10′ (Co)	Toluene	2.0043	—	3.11	—	3
11′ (Ni)	Toluene	2.0042	3.10	0.70	—	3

[a] Weak broad signal was registered.

suggest that the coordination number for the divalent Zn–chloride complex is five with distorted trigonal bipyramidal geometry, as it was found by X-ray crystallography (Fig. 1).

The spectrum of Co complex **5** displays low intensive long wave bands at 487, 546, 611 nm usually attributable to characteristic $^4E''(P) \leftarrow {}^4A'_2(F)$, $^4A'_2\ (P) \leftarrow {}^4A'_2(P)$ transitions of high spin d^7 Co(II) complexes.[26,27] The spectrum of Co complex **10** indicates different absorptions at 403 and 520 nm that demonstrate the influence of a ligand X on the molecular orbitals of the complex. The electron spectrum of the Ni complex **6** shows d–d bands at 381 and 634 nm ($^3E \leftarrow {}^3B_1$). The spectrum points out a five-coordinated metal having a N_3Cl_2 donor set in a distorted bipyramidal complex. The bands corresponding to d–d transitions in Ni acetate complex **11** were found at 385 and 596 nm.

The electron spectra of the Fe complexes **4** and **9** show long waves d–d bands at 385, 419 (**4**), and 495, 680 nm (**9**), respectively. The spectra confirm a distorted octahedral geometry.

ESR spectra

The chemical oxidation of the phenol containing compounds **1–11** was carried out in toluene using lead dioxide in vacuumed tubes yielding phenoxyl radicals **1′–11′** and it was monitored by ESR method. The X-band ESR spectra measured at 293 K show the spin density distribution in the organic ligand. The isotropic *g*-value for the radicals **1′–11′** are varied in the range of 2.0030–2.0049. The parameters of the ESR spectra of radicals are listed in Table 2.

The ESR spectra of radicals are multiplets corresponding to the coupling of the unpaired electron with two equivalent *meta*-protons of the phenoxyl ring (^1H, $S = 1/2$), protons of CH_2 and amine nitrogen atom (^{14}N, $S = 1$). The experimental and simulated ESR spectra (Fig. 4) of radical **1′** exhibit 15 lines corresponding to the coupling of the unpaired electron with paramagnetic nuclei ^1H and ^{14}N.

The stability of phenoxyl radicals is influenced by the nature of the metal in the complex. The most intensive signals were found for more stable radicals formed from ligand **1**, Zn and Fe complexes. The radical **1′** is stable at room temperature in the absence of dioxygen for several days. The presence of

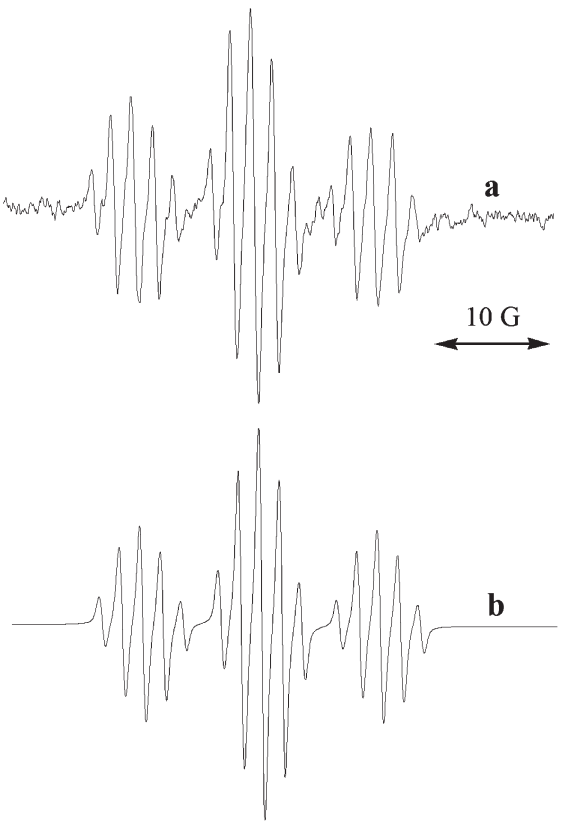

Fig. 4 Experimental (toluene, PbO_2, 290 K) (a) and simulated (b) ESR spectra of radical **1′** with parameters $g = 2.0030$; $a_N = 1.90$ (1N), $a_H = 10.89$ (2H), $a_H = 1.82$ (2H); $\Gamma = 0.60$ G, $L/G = 0.30$ (b).

Co, Mn and Ni ions in complexes leads to other radical products during oxidation by PbO_2, probably due to the ligand destruction.

Previously a number of analogues of phenoxyl radicals generated in the oxidation of the corresponding substituted benzylamines have been studied.[28,29] We observed that most of the organometallic and coordination compounds based on 2,6-di-*tert*-butylphenol undergo intramolecular transformations or destruction upon the change of ligand magnetic state. The stability and the values of the hyperfine splitting

constants of these radicals are influenced by the electron-withdrawing or electron-donating character of the *para*-substituent in the phenyl ring. In general, the coordination group between M and the phenoxyl moiety serves as a mediator of electronic interactions. The main factors that influence intramolecular electron transfer (IET) are: (1) conjugation between the phenoxyl and metal; (2) the distance between the radical center and metal; (3) the nature of the paramagnetic metal nucleus; (4) temperature. The introduction of a transition metal in most cases increases the stability of the phenoxyl radicals. There are few examples of stable organometallic phenoxyls with strong magnetic interaction, among them the strongest interaction a_M 94 G (M = ^{195}Pt) was observed for transition metals (Pt, Pd) linked through the σ bond to the *para*-position of phenoxyl.[30] The analogues of DPA complexes are porphyrins. The ESR spectra of the phenoxyl radicals attached to metalloporphyrins (M = Zn, Fe, Co, Cu, Ni, Pt, Pd) were registered as triplets indicating only coupling between the unpaired electron and the *meta*-protons of the phenoxyl ring a_{2H} 1.5–1.8 G.[20]

In the present work the absence of IET between radical and metal could be explained by the absence of phenol ring conjugation with the bis(2-pyridylmethyl) fragment and metal.

The ferrocene unit, for instance, with an Fe(II) center is an electron-donating group and increases the stability of radicals as has been shown by ESR.[31]

DPPH radical scavenging activity

The presence of a 3,5-di-*tert*-butyl-4-hydroxyphenyl substituent linked to the DPA ligand in the metal complexes allows the suggestion that these compounds might display antioxidant properties. Since the compounds act by the mechanism of hydrogen atom abstraction from the phenol moiety and produce quite stable phenoxyl radicals one could expect they would show a high antioxidant capacity. The scavenging activity has been studied in the process of hydrogen atom transfer to the stable free radical 2,2-diphenyl-1-picrylhydrazyl (DPPH).[32] This radical is a useful reagent for the investigation of the radical scavenging activity of phenols, catecholes, *etc.*[33] The accepted reaction mechanism is abstracting a hydrogen atom from a phenol donor to give diphenylpicrylhydrazine and phenoxyl radical. The reaction involves a color change from violet to yellow, which can be monitored spectrophotometrically by measuring the decrease in absorbance at 517 nm (Fig. 5).

The results of the DPPH test at 20 °C shows that the activity depends strongly upon the metal in the compounds and in the series of compounds **2–11** the activity was found to be highest for Mn complexes **3** and **8** (EC_{50} = 70 ± 2 and 40 ± 2 μM, respectively). The EC_{50} value of ligand **1** was found to be similar (50 ± 1 μM) whereas the activity of other complexes was at least one order lower (Table 3). The EC_{50} parameter indicates the reactivity of a compound toward DPPH, giving restricted information on the mechanistic outcome of the reaction. The reaction followed second-order kinetics, the rate constants k were obtained from a plot of 1/[DPPH] *vs.* time. Linear regression (r^2 > 0.99) gave the parameter k as a slope of the

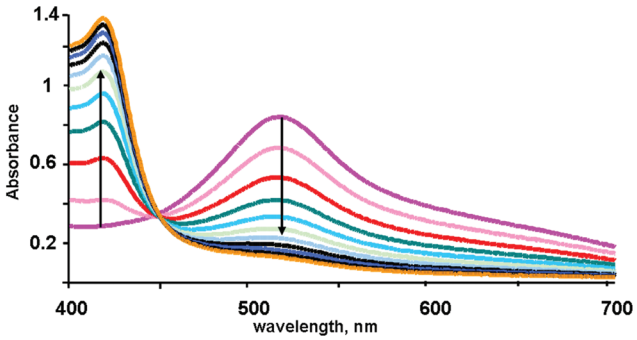

Fig. 5 Changes in UV-vis spectrum of DPPH (0.1 M) in the presence of ligand **1** (0.05 M) during 30 min in MeOH, 293 K.

Table 3 The values of EC_{50} and k in DPPH test (MeOH, 20 °C) and inhibition data in linoleic acid peroxidation, lipoxygenase (LOX) and Cu^{2+} reducing activity in Trolox-equivalents in the presence of **1–11**

	DPPH test				
N (M)	EC_{50} (μM)	k (L mol^{-1} s^{-1})	Inhibition of linoleic acid[a] (%)	LOX inhibition IC_{50} (μM)	$TEAC_{CUPRAC}$
1 (L)	50 ± 1	13.5	54	79.8 ± 1.9	0.24 ± 0.01
2 (Zn)	>500	0.65	49	41.1 ± 3.2	0.07 ± 0.03
3 (Mn)	70 ± 2	15.3	60	33.6 ± 2.1	0.17 ± 0.01
4 (Fe)	100 ± 5	[b]	29	39.0 ± 2.0	0.77 ± 0.03
5 (Co)	230 ± 5	2.1	27	31.6 ± 1.6	0.07 ± 0.01
6 (Ni)	450 ± 10	0.3	20	29.7 ± 1.8	0.09 ± 0.01
7 (Zn)	350 ± 6	0.7	46	35.2 ± 3.1	0.07 ± 0.03
8 (Mn)	40 ± 2	17.7	61	24.9 ± 2.2	0.18 ± 0.02
9 (Fe)	>500	4.6	38	26.6 ± 2.0	0.31 ± 0.01
10 (Co)	>500	2.3	48	28.7 ± 1.9	0.09 ± 0.01
11 (Ni)	>500	0.5	46	32.2 ± 2.0	0.08 ± 0.01

[a] Concentration of test compound was 2 mM, 20 °C. [b] The rate of reaction was too high to be determined distinctly.

curve (Fig. 6, Table 3). For ligand **1** at equimolar ratio with DPPH 1 : 1 and initial concentration of 0.1 mM k = 13.5 L mol^{-1} s^{-1} was found.

Thus, the rate constants were found to depend on the metal incorporated in the complex. The most active reducing agent was complex **4**, probably due to the presence of readily oxidizable Fe^{2+}. The acetate anion in **9** complicated the DPPH reduction. In other metal complexes the influence of the anion is not well pronounced.

Inhibitory activity in linoleic acid peroxidation

In order to expand the study of the radical scavenging activity of compounds **1–11** the radical chain process of peroxidation of unsaturated fatty acids has been used with the example of linoleic acid as a model substrate for lipid peroxidation. The peroxidation has been induced by Fe^{2+} ions and carried out at 37 °C in the presence of 2 mM of the compounds under investigation and dioxygen as an oxidant. The monitoring of linoleic acid peroxidation level was performed by the determination of the total concentration of thiobarbituric acid reactive substances (TBARS).

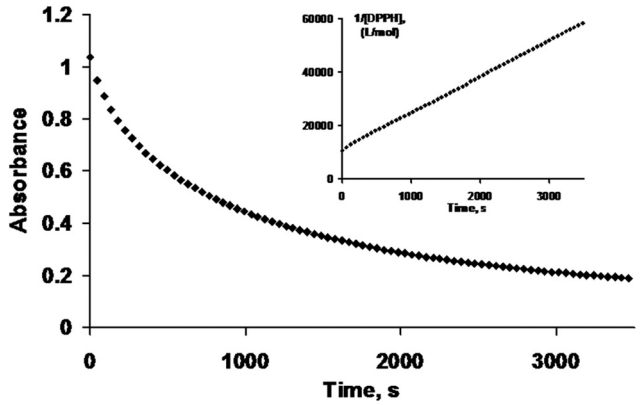

Fig. 6 Reaction of DPPH (0.1 M) with **1** (0.1 M), monitored at 517 nm in MeOH, 293 K. The insertion: plot of 1/[DPPH] *vs.* time for the reaction of DPPH and **1** in MeOH.

Comparing with the data of the control experiment without any additives the inhibition percentage was calculated (Table 3). The complexes of Mn **3** and **8** and ligand **1** show the activity in the inhibition of radical chain oxidation >50%. It should be pointed out that the iron complexes **4** and **9** possess low activity. It may be that the iron site in the molecules of **4** and **9**, which is capable of one-electron transfer, acts as a pro-oxidant under experimental conditions and it can promote free radical chain oxidation of the unsaturated fatty acid as a model substrate of lipid peroxidation.

Cu^{2+} ion reducing (CUPRAC) assay. The one-electron transfer capacity of compounds **1–11** has been examined as the ion Cu^{2+} ion reducing ability, the method proposed by Apak *et al.* that was used with slight modification.[34] The kinetics of copper(II) reduction by metal complexes was not detected spectrophotometrically. The results show that there is significant activity among the studied compounds that have iron complexes only (Table 3). Thus, the iron complexes exhibit strong electron transfer capacity. The main role of the metal ion is experimentally proved. To confirm this hypothesis, additional experiments were provided with the participation of ferrous salts – chloride and acetate. Results were presented in Trolox-equivalents (TEAC CUPRAC – Trolox equivalent antioxidant capacity). The comparison of the obtained TEAC CUPRAC values allows the conclusion that the ligand does not play any significant role in electron transfer to the metal ion. Comparing the ability of ferrous salts to transfer electrons (TEAC CUPRAC for $FeCl_2$ and $Fe(OAc)_2$ are 0.78 and 0.06, respectively), it is obvious that in the form of chloride the iron complex reduces the copper ion as effectively as iron salt does it. Comparison of the other metal complexes shows overall low capacity for electron transfer and a counter-ion has no significant effect on the activity.

Lipoxygenase inhibitory assessment. During oxidative stress lipoxygenase (LOX) can exhibit uncontrolled activity and may cause cell membrane destruction by phospholipids oxidation. Thus, lipoxygenase inhibition under pathologic conditions decreases the total level of oxidative stress.[35] The LOX inhibition activity of the studied compounds was estimated in order to determine the capacity of compounds of decreasing oxidative stress level. IC_{50} values for each compound (Table 3) were calculated graphically using data from experiments in the presence of different concentrations of compounds **1–11**.

All compounds demonstrate IC_{50} values lower than 50 μM and can be considered as potential lipoxygenase inhibitors. There was no significant difference between the inhibitory activities of chloride or acetate metal complexes. Ligand **1** is the weakest inhibitor, which proves the key role of the metal in inhibitory activity.

Superoxide radical anion scavenging activity

Reactive oxygen species (ROS) are produced during normal cellular metabolism and assist in many biochemical processes. The cells protection from ROS at the normal metabolism is realized by antioxidative defense enzymes such as superoxide dismutase (SOD) and catalase. The superoxide anion $O_2^{\cdot -}$ may cause different heavy effects, leading to tissue injury and inflammation.[36] SOD represents the first line of defense against $O_2^{\cdot -}$. SOD catalyzes the dismutation of superoxide anion to O_2 and hydrogen peroxide. It plays a protective effect in the models of several diseases. However, the use of the native SOD has several restrictions related with low cell permeability and short half-life.[37] Synthetic therapeutic antioxidants (catalytic oxidants) such as SOD mimics with a broad range of antioxidant activity can solve the problem of cell defense system from reactive biological oxidants.[38] The superoxide radical-anion scavenging activity of the complexes was determined by NBT assay[39] In this method $O_2^{\cdot -}$ generated by the xanthine–xanthine oxidase (X–XO system) reduces yellow nitro blue tetrazolium (NBT) to the blue formazan, which is measured spectrophotometrically at 560 nm. Therefore, compounds can compete with NBT for oxidation of the generated superoxide radical-anion. Scavengers are able to inhibit the formation of blue formazan. The kinetic curves of blue formazan formation in the presence of complex **4** are shown in Fig. 7.

All complexes **2–11** demonstrate the ability to scavenge the $O_2^{\cdot -}$, with IC_{50} values in the micromolar range (Table 4).

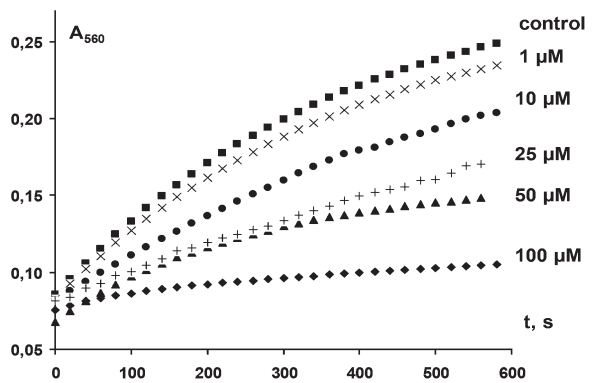

Fig. 7 Kinetic curves of formazan formation in the system NBT–xanthine–xanthine oxidase in the presence of different concentrations of Fe complex **4**.

Table 4 Superoxide radical-anion scavenging activity of compounds **1–11** in the xanthine–xanthine oxidase test

	Inhibition (%)		
N (M)	10 μM	100 μM	IC_{50} (μM)
1 (L)	0.70 ± 0.05	6.0 ± 1.9	[a]
2 (Zn)	13.0 ± 2.2	52.0 ± 2.1	91
3 (Mn)	83.0 ± 0.5	98.0 ± 1.1	2
4 (Fe)	40.0 ± 0.9	82.0 ± 0.7	15
5 (Co)	2.5 ± 1.4	61.0 ± 0.8	81
6 (Ni)	20.0 ± 1.3	31.0 ± 1.7	[a]
7 (Zn)	1.7 ± 0.5	5.0 ± 2.2	[a]
8 (Mn)	85.0 ± 0.7	99.0 ± 0.5	0.5
9 (Fe)	1.4 ± 1.9	2.5 ± 2.4	[a]
10 (Co)	19.0 ± 1.1	24.0 ± 1.5	[a]
11 (Ni)	2.0 ± 0.5	7.0 ± 1.9	[a]

[a] Inhibition activity of compound is less than 50%.

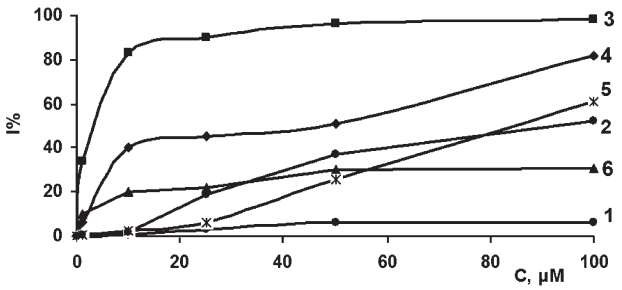

Fig. 8 Scavenging activity of the ligand **1** and complexes **2–6** toward the superoxide radical-anion generated in the X–XO system.

However, the most active inhibitors were found to be chloride **3** (Mn) followed by **4** (Fe) > **5** (Co) > **2** (Zn) > **6** (Ni) > **1** (L) at the concentration of 100 μM (Fig. 8). The scavenging effect of other metal acetates on the superoxide radical-anion decreases in the order: **8** (Mn) ≫ **10** (Co) > **11** (Ni) > **7** (Zn) > **9** (Fe) at the concentration of 100 μM. In the series of acetates, Mn complex **8** was the best inhibitor.

These results indicate that manganese complexes possess the highest superoxide radical-anion scavenging activity in a series of other metal complexes. Moreover, the ligand X also influences the activity. The chloride complexes are more effective inhibitors than acetates and have lower IC_{50} values.

On the contrary, the value of inhibition percentage in the presence of 100 μM ligand **1** (6.0 ± 1.9%) proves that the ligand does not possess any significant activity in the interaction with superoxide radical-anion. Thus, it was found that the nature of the metal plays a critical role in superoxide scavenging activity of the complexes.

Evaluation of complexes influence on lipids peroxidation in rat brain homogenates

Oxidative stress is one of the major mechanisms implicated in a variety of diseases; in particular, neurodegenerative diseases, including stroke, Alzheimer's disease, and Parkinson's disease.[40,41] The molecular mechanisms of pathogenetic processes implicated in oxidative stress include free radical stages of membrane damage. They include intensification of lipid peroxidation (LP) of biological membranes, which can be determined as an increase in the content of TBARS. The increase of TBARS including lipid hydroperoxides and aldehydes in biological samples is a result of oxidative stress. In practice, TBARS are expressed in terms of malondialdehyde (MDA) equivalents. The comparative study of activity of a series of complexes in lipid peroxidation has been carried out using rat brain homogenates (RBH). We studied lipid peroxidation induced by Fe^{3+}-ions ($FeNH_4(SO_4)_2{\cdot}12H_2O$) or by *tert*-butylhydroperoxide (^{t}BHP). All the experiments were repeated using four different preparates of RBH. Data are normalized between the control probe with oxidant (100%) and blank probe with only diluent (0%). The values are expressed as mean % ± SD in Table 5.

Table 5 Effect of complexes (10 μM) on induced LP of RBH, estimated as TBARS

	Inhibition of LP, induced by Fe^{3+}	Level of RBH LP in the presence of 10 μM of compound (%)	
Compound	IC_{50} (μM)	Fe^{3+}-induced LP	^{t}BHP-induced LP
1 (L)	0.4 ± 0.1	13.6 ± 1.2	94.8 ± 5.3
2 (Zn)	3.6 ± 0.1	10.2 ± 0.5	86.6 ± 0.7
3 (Mn)	nd[b]	14.1 ± 0.5	73.2 ± 5.9
4 (Fe)	nd[b]	12.9 ± 0.9	[a]
5 (Co)	2.5 ± 0.1	17.6 ± 1.4	65.8 ± 4.8
6 (Ni)	5.1 ± 0.1	10.2 ± 0.3	78.0 ± 12.0
7 (Zn)	1.9 ± 0.1	10.7 ± 0.5	84.1 ± 4.2
8 (Mn)	nd[b]	13.5 ± 0.6	74.3 ± 4.0
9 (Fe)	nd[b]	14.1 ± 0.7	[a]
10 (Co)	2.6 ± 0.1	17.9 ± 0.6	67.4 ± 10.4
11 (Ni)	8.7 ± 0.1	10.8 ± 0.6	85.9 ± 5.4

[a] Complex with pro-oxidant activity – the peroxidation level is higher than that of control experiment. [b] nd – not determined.

One can see from Table 5 that all the compounds are highly effective inhibitors of Fe^{3+} induced LP. However, they have shown low activity against ^{t}BHP induced LP. It should be noted that Fe complexes significantly increased ^{t}BHP induced LP. It seems to be related to oxidation of Fe^{2+} in the complex to Fe^{3+}, which could be additional promoters of LP.

Conclusions

The synthesis, structures, redox properties and *in vitro* antioxidant effects of a series of new Mn, Fe, Co, Ni, Zn, Cu complexes with [*N*-(3,5-di-*tert*-butyl-4-hydroxybenzyl)-*N*,*N*-di-(2-pyridylmethyl)]amine is presented. The metal complexes **2–11** are polytopic agents since their molecules possess both organic antioxidant phenol groups capable of hydrogen atom transferring and a transition metal center that is capable of electron transfer.

The oxidation of the compounds leads to the formation of phenoxyl radicals in the ligand environment and was

investigated by ESR. The relatively stable paramagnetic species formed in the redox transformations are ligand-centered phenoxyl radicals.

The antioxidant radical scavenging activity of complexes was measured using DPPH-test and linoleic acid peroxidation. The highest activity was found for Mn complexes in both tests.

In electron transfer reactions (CUPRAC test and inhibition of enzymatic generation of superoxide radical-anion by xanthine oxidase) Mn complexes possess an activity higher than that of other metal complexes. The LOX inhibition activity of the studied compounds was evaluated. All compounds demonstrate IC_{50} values lower than 50 μM and can be considered as potential lipoxygenase inhibitors.

The *in vitro* biological experiments, which were performed by using rat brain homogenate, indicate high antioxidant activity of all the compounds studied. This result opens up the possibility for the design of novel biomimetic systems that might serve as electron and proton transfer agents in biological systems.

Experimental

Materials and equipment

The starting 2,6-di-*tert*-butylphenol, di-(2-picolyl)amine (97% Aldrich) and metal salts were commercially available and used as supplied. $CDCl_3$ (Merck) was used without further purification; other solvents were routinely distilled prior to use. Elemental analyses were performed in the Laboratory of Microanalysis at the Moscow State Lomonosov University (Moscow), Russia.

Infrared spectra were recorded in KBr pellets or in CH_2Cl_2 solution with a "IR200 Thermo Nicolet" spectrometer. Electronic absorption spectra were measured on a "Evolution 300 Termo Scientific" spectrophotometer.

The NMR measurements were performed with a Bruker Avance-400 spectrometer operating on 400.1 (^{1}H) and 100.6 MHz (^{13}C) in $CDCl_3$.

The MALDI TOF spectra were acquired using a Autoflex II (Bruker daltonics) mass spectrometer. The samples were dissolved in $CHCl_3$ and put at target.

ESR spectra were recorded with Bruker EMX spectrometer at X-band frequency (9.8 GHz). The measurements were carried out after pre-evacuation (10^{-2} Torr) of tubes with solutions of samples (concentration 1×10^{-4} M). The oxidant PbO_2 (Aldrich) was taken in a tenfold excess.

Syntheses

Ligand L (1). To a solution of CH_2O in H_2O (37%, 0.32 mL, 4.0 mmol) in 1 mL of EtOH, the solution of di-2-picolylamine (0.72 mL, 4.0 mmol) in 0.5 mL of EtOH was added, the suspension was stirred at 0 °C for 30 min, then 2,6-di-*tert*-butylphenol (0.82 g, 4.0 mmol) in 2 mL of EtOH was added and stirred at 20 °C for 1 h. The resulting mixture was refluxed for 4 h and left overnight. The solution was added to 100 mL of 0.01 M HCl, and the mixture was washed by ether. To water solution the 1 M KOH and 10 mL of ether was added, white product was repeatedly extracted by a new portion of KOH and ether. The ether extract was dried over $CaCl_2$. The solvent was partially removed in vacuum and the solution left for crystallization on the air. White crystals of **1** were washed by a small amount of ether and dried in the air. Yield 1.11 g (67%). Mp 129–130 °C. $C_{27}H_{35}N_3O$: Anal. calcd: C, 77.66; H 8.45; N 10.06. Found: C 77.74; H 8.52; N 9.91%. IR (KBr pellet, cm^{-1}): 1431 (s), 1593 (s), ν(CH) 2825–3010 (s) ν(OH associated) 3293 (w), 3511 (w) ν(OH). MS (MALDI TOF), *m*/*z*: 440 $[C_{27}H_{35}N_3ONa]^+$ (M + Na)$^+$.

^{1}H-NMR (δ (ppm), $CDCl_3$): 1.45 (s, 18 H, C(CH_3)$_3$); 3.62 (s, 2H, CH_2–Ar); 3.85 (s, 4H, N(CH_2)$_2$)); 5.14 (s, 1 H, O*H*); 7.14 (t, 2H, $^3J_{HH}$ = 6.7 Hz, 2 Py); 7.21 (s, 2H, C$_6H_2$); 7.61–7.70. (m, 4 H, 2 Py); 8.52 (d, 2H, $^3J_{HH}$ = 5.1 Hz, 2 Py). ^{13}C-NMR: 30.35 (C(*C*H$_3$)$_3$); 34.31 (*C*C(CH$_3$)$_3$); 58.73 (*C*H$_2$–Ar); 60.12 ((Ar*C*H$_2$)$_2$N–); 121.85; 122.65; 125.63; 129.37; 135.63; 136.33; 148.90; 152.74; 160.19 (C-arom). UV-vis spectrum (MeOH), λ_{max}/nm (ε, M^{-1} cm^{-1}): 263 (7296), 268 sh; 283 sh.

[$ZnCl_2$L] (2). To a solution of **1** (209 mg, 0.5 mmol) in 3 mL of ethanol, $ZnCl_2 \cdot 2H_2O$ (86 mg, 0.5 mmol) in 0.6 mL of ethanol was added under stirring. The white crystals that appeared in several seconds were left to crystallize for 1 h. The crystals were filtered, washed with EtOH and dried in the air. Yield 220 mg (79%). Mp. >250 °C. $C_{27}H_{35}N_3OZnCl_2$: Anal. calcd: C, 58.55; H 6.37; N 7.59. Found: C 58.29; H 6.33; N 7.40%. IR (KBr pellet, cm^{-1}): 1446 (s), 1604 (s), ν(CH) 2869–2956 (s), ν(OH non-associated) 3618 (w). MS (MALDI TOF), *m*/*z*: 516 $[C_{27}H_{35}N_3OZnCl]^+$ (M − Cl)$^+$. ^{1}H-NMR (δ (ppm), $CDCl_3$): 1.41 (s, 18 H, C(CH_3)$_3$); 3.62 (s, 2H, CH_2–Ar); 4.14 (s, 4H, N(CH_2)$_2$); 5.26 (s, 1 H, O*H*); 6.80 (s, 2H, Ar); 7.26 (d, 2H, $^3J_{HH}$ = 7.8 Hz, 2 Py); 7.46–7.53 (m, 2 H, Py); 7.86–7.94 (m, 2H, Py); 9.26 (d, 2H, $^3J_{HH}$ = 5.0 Hz, 2 Py). ^{13}C-NMR: 30.22 (C(*C*H$_3$)$_3$); 34.23 (*C*C(CH$_3$)$_3$); 55.32 (*C*H$_2$–Ar); 55.74 ((Ar*C*H$_2$)$_2$N–); 122.08; 123.22; 124.51; 127.88; 135.95; 136.64; 149.91; 153.68; 153.98 (C-arom). UV-vis spectrum (MeOH), λ_{max}/nm (ε, M^{-1} cm^{-1}): 262.5 (9556); 269.5 sh. The crystals of **2** were suitable for single-crystal X-ray structure determination.

[$MnCl_2$L] (3). To a solution of **1** (250 mg, 0.6 mmol) in 1 mL of MeOH $MnCl_2 \cdot 4H_2O$ (118 mg, 0.6 mmol) was added under stirring. The white crystals that appeared in several seconds were left to crystallize for 15 min. The crystals were filtered, washed with MeOH and dried in the air. Yield 279 mg (80%). Mp. (dec.) 246–250 °C. $C_{27}H_{39}N_3O_3MnCl_2$: Anal. calcd: C, 55.95; H 6.73; N 7.25. Found: C 56.60; H 6.79; N 7.37%. IR (KBr pellet, cm^{-1}): 1446 (s), 1604 (s), ν(CH) 2869–2956 (s), ν(OH associated) 3467–3523 (s), ν(OH non-associated) 3617 (w). MS (MALDI TOF), *m*/*z*: 507 $[C_{27}H_{35}N_3OMnCl]^+$ (M − Cl − 2H_2O)$^+$. UV-vis spectrum (MeOH), λ_{max}/nm (ε, M^{-1} cm^{-1}): 232.5 sh; 257.5 sh; 262.5 (8908); 268.5 sh. The crystals of **3** were suitable for single-crystal X-ray structure determination.

[$FeCl_2$L] (4). To a solution of **1** (210 mg, 0.5 mmol) in 1 mL of EtOH, $FeCl_2$ (64 mg, 0.5 mmol) in Ar atmosphere was added under stirring. The mixture was stirred for 5 min. The solvent was removed under reduced pressure, the yellow powder was washed with hexane and dried in the air. Yield 246 mg (90%).

Mp. (dec.) 200 °C. $C_{27}H_{35}N_3OFeCl_2$: Anal. calcd: C, 59.58; H 6.48; N 7.72. Found: C 59.40; H 6.48; N 7.79%. IR (KBr pellet, cm^{-1}): 1434 (s), 1606 (s), ν(CH) 2844–3000 (s), ν(OH non-associated) 3667 (s). MS (MALDI TOF), *m*/*z*: 508 $[C_{27}H_{39}N_3O_3FeCl]^+$ (M − Cl)$^+$. UV-vis spectrum (MeOH), λ_{max}/nm (ε, M^{-1} cm^{-1}): 233 sh; 258 (9401); 281 sh; 385 (1422), 419 sh.

[$CoCl_2$L] (5). To a solution of **1** (210 mg, 0.5 mmol) in 2 mL of MeOH, $CoCl_2{\cdot}6H_2O$ (119 mg, 0.5 mmol) was added under stirring. The purple crystals that appeared in several seconds were left to crystallize for 15 min. The crystals were filtered, washed with MeOH and dried in the air. Yield 165 mg (60%). Mp. (dec.) >250 °C. $C_{27}H_{35}N_3OCoCl_2$: Anal. calcd: C, 59.24; H 6.44; N 7.68. Found: C 59.12; H 6.67; N 7.51%. IR (KBr pellet, cm^{-1}): 1434 (s), 1608 (s), ν(CH) 2844–3000 (s), ν(OH non-associated) 3637 (s). MS (MALDI TOF), *m*/*z*: 511 $[C_{27}H_{35}N_3OCoCl]^+$ (M − Cl)$^+$. UV-vis spectrum (MeOH), λ_{max}/nm (ε, M^{-1} cm^{-1}): 262.5 (6956); 269 sh; 281.5 sh; 487, 546 (41), 611.

[$NiCl_2$L] (6). The mixture of **1** (210 mg, 0.5 mmol) and $NiCl_2{\cdot}6H_2O$ (119 mg, 0.5 mmol) in 5 mL of acetone was refluxed for 1 h. The light green crystals were left to crystallize for 15 min at room temperature. The crystals were filtered, washed with acetone and dried in the air. Yield 207 mg (75%). Mp. (dec.) >255 °C. $C_{27}H_{35}N_3ONiCl_2$: Anal. calcd: C, 59.21; H 6.39; N 7.67. Found: C 59.32; H 6.64; N 7.42%. IR (KBr pellet, cm^{-1}): 1434 (s), 1608 (s), 1702 (s), ν(CH) 2848–2998 (s), ν(OH non-associated) 3635 (w). MS (MALDI TOF), *m*/*z*: 510 $[C_{27}H_{35}N_3ONiCl]^+$ (M − Cl)$^+$. UV-vis spectrum (MeOH), λ_{max}/nm (ε, M^{-1} cm^{-1}): 233.5; 256; 261 (7842); 269 sh; 281 sh; 387; 634 (10).

[$Zn(OAc)_2$L] (7). The mixture of **1** (209 mg, 0.5 mmol) and $Zn(OAc)_2{\cdot}2H_2O$ (110 mg, 0.5 mmol) in 3 mL of acetone was refluxed for 1 h. The white crystals were filtered, washed with acetone and dried in the air. Yield 220 mg (73%). Mp. >235 °C. $C_{31}H_{41}N_3O_5Zn$: Anal. calcd: C, 61.94; H 6.88; N 6.99. Found: C 61.77; H 6.83; N 7.05%. IR (KBr pellet, cm^{-1}): 1432 (s), 1577 (s), ν(CH) 2867–3002 (s), ν(OH non-associated) 3631 (w). MS (MALDI TOF), *m*/*z*: 540 $[C_{29}H_{38}N_3OZn]^+$ (M − OAc)$^+$. ^{1}H-NMR (δ (ppm), $CDCl_3$): 1.42 (s, 18 H, C(CH_3)$_3$); 2.00 (s, 6 H, CH_3CO); 3.60 (s, 2H, CH_2–Ar); 4.18 (s, 2H, NCH_2); 4.27 (s, 2H, NCH_2); 5.43 (s, 1 H, O*H*); 6.75 (s, 2H, Ar); 7.28 (m, 2H, Py); 7.48 (m, 2H, Py); 7.89 (m, 2H, Py); 8.90 (m, 2H, Py). ^{13}C-NMR: 23.31 (CH_3CO); 30.30 (C(CH_3)$_3$); 34.28 (CC(CH$_3$)$_3$); 55.17 (CH_2–Ar); 55.81 ((ArCH_2)$_2$N–); 122.08; 123.07; 124.45; 128.17; 136.06; 139.26; 149.45; 154.01, 154.55; (C-arom); 182.22 (C═O). UV-vis spectrum (MeOH), λ_{max}/nm (ε, M^{-1} cm^{-1}): 231; 256; 262.5 (10355); 269.5 sh; 281.5 sh.

[$Mn(OAc)_2$L] (8). To a solution of **1** (210 mg, 0.5 mmol) in 3 mL of acetone, $Mn(OAc)_2{\cdot}4H_2O$ (122 mg, 0.5 mmol) was added under stirring, and the mixture was refluxed for 1 h. The colorless crystals, after cooling to room temperature, were filtered off, washed with acetone and dried in the air. Yield 266 mg (85%). Mp. (dec.) 180–185 °C. $C_{31}H_{41}N_3O_5Mn$: Anal. calcd: C, 63.05; H 7.00; N 7.12. Found: C 63.16; H 7.12; N 7.16%. IR (KBr pellet, cm^{-1}): 1433 (s), 1577 (s), 1604 (s), ν(CH) 2868–3002 (s), ν(OH associated), 3631 (w)ν(OH non-associated). MS (MALDI TOF), *m*/*z*: 514 $[C_{29}H_{38}N_3O_3Mn]^+$ (M − OAc)$^+$. UV-vis spectrum (MeOH), λ_{max}/nm (ε, M^{-1} cm^{-1}): 232.5 sh; 57.5 sh; 262.5 (8919); 268.5 sh.

[$Fe(OAc)_2$L] (9). The mixture of **1** (210 mg, 0.5 mmol) and $Fe(OAc)_2$ (87 mg, 0.5 mmol) in 3 mL of acetonitrile in Ar atmosphere was stirred for 1 h. The solvent was removed under reduced pressure; the brown residue was washed with hexane and dried in the air. Yield 222 mg (75%). Mp. (dec.) 150 °C. $C_{31}H_{41}N_3O_5Fe$: Anal. calcd: C, 62.95; H 6.99; N 7.10. Found: C 63.14; H 6.96; N 7.25%. IR (KBr pellet, cm^{-1}): 1433 (s), 1556 (s), ν($COCH_3$) 1587 (s), ν(CH) 2856–3002 (w), ν(OH associated) 3428-(wide, w), ν(OH non-associated) 3627 (w). MS (MALDI TOF), *m*/*z*: 532 $[C_{29}H_{38}N_3O_3Fe]^+$ (M − OAc)$^+$. UV-vis spectrum (MeOH), λ_{max}/nm (ε, M^{-1} cm^{-1}): 262.5 (13 860); 419.5 (1645); 495 (371) sh, 680 sh.

[$Co(OAc)_2$L] (10). To a solution of **1** (210 mg, 0.5 mmol) in 5 mL of acetone, $Co(OAc)_2{\cdot}4H_2O$ (124 mg, 0.5 mmol) was added and refluxed for 1 h. The pink crystals were filtered, washed with acetone and dried in the air. Yield 175 mg (59%). Mp. (dec.) 205 °C. $C_{31}H_{41}N_3O_5Co{\cdot}0.5\ H_2O$: Anal. calcd: C, 61.69; H 7.01; N 6.96. Found: C 61.39; H 7.19; N 6.74%. IR (KBr pellet, cm^{-1}): 1446 (s), ν($COCH_3$) 1594 (s), ν(CH) 2867–3002 (s), ν(OH associated) 3338–3450 (s), ν(OH non-associated). MS (MALDI TOF), *m*/*z*: 535 $[C_{29}H_{38}N_3O_3Co]^+$ (M − OAc)$^+$. UV-vis spectrum (MeOH), λ_{max}/nm (ε, M^{-1} cm^{-1}): 230 (8232); 262 (6236); 403 (127); 520 (60).

[$Ni(OAc)_2$L] (11). To a solution of **1** (210 mg, 0.5 mmol) in 6 mL of acetone, $Ni(OAc)_2{\cdot}4H_2O$ (125 mg, 0.5 mmol) was added and refluxed for 1 h. The pale blue crystals were filtered, washed with acetone and dried in the air. Yield 205 mg (69%). Mp. (dec.) >250 °C. $C_{31}H_{41}N_3O_5Ni{\cdot}0.5\ H_2O$: Anal. calcd: C, 61.71; H 7.02; N 6.96. Found: C 61.41; H 7.14; N 6.82%. IR (KBr pellet, cm^{-1}): 1448 (s), 1583 (s), 1606 (s), ν(CH) 2869–3004 (s), ν(OH associated) 3300–3500 (s), ν(OH non-associated) 3629 (w), 3677 (w). MS (MALDI TOF), *m*/*z*: 534 $[C_{29}H_{38}N_3O_3Ni]^+$ (M − OAc)$^+$. UV-vis spectrum (MeOH), λ_{max}/nm (ε, M^{-1} cm^{-1}): 233.5; 256.5; 261 (6810); 268.5 sh; 385, 600 (11).

Crystallographic data collection and structure determination

Single crystals were grown from EtOH solution. All diffraction data were collected on a Bruker SMART APEX II CCD diffractometer [λ(MoKα) = 0.71072 Å, ω-scans] at 100 K. The substantial redundancy in data allows empirical absorption correction to be performed with SADABS, using multiple measurements of equivalent reflections. The structures were solved by direct methods and refined by the full-matrix least-squares technique against F^2 in the anisotropic–isotropic approximation. The hydrogen atoms were located from difference electron density syntheses and refined in a rigid body model. Analysis of Fourier maps in both structures allowed one to reveal about 8–10 peaks of residual electron density (1.2–3.1% e × A^{-3}) in cavities between complexes. These peaks can be considered as the superposition of several C_2H_5OH molecules with different occupation values. We could not establish an appropriate model for refining the above residual electron density. Thus,

Table 6 Crystal data and structure refinement parameters for **2**, **3**

Complex	$[ZnCl_2L]$ **2**	$[MnCl_2L]$ **3**
Empirical formula	$C_{29}H_{41}Cl_2ZnN_3O_2$	$C_{29}H_{41}Cl_2MnN_3O_2$
Fw	599.92	589.49
Temp [K]	100	100
Cryst syst	Monoclinic	Monoclinic
Space group	$P2_1/n$	$P2_1/n$
a (Å)	14.579(3)	14.9561(15)
b (Å)	13.032(3)	13.1472(14)
c (Å)	16.021(3)	16.190(2)
β (°)	106.13(3)	105.619(3)
V (Å^3)	2924.1(10)	3065.8(6)
Z (Z')	4 (1)	4 (1)
F(000)	1264	1244
d_{calc} (g cm^{-1})	1.363	1.277
μ (cm^{-1})	10.53	6.34
$2\theta_{max}$ (°)	58	58
Reflns collected	34536	34470
Independent reflns (R_{int})	7784 (0.0408)	8154 (0.0345)
Observed reflns [$I > 2\sigma(I)$]	6335	6887
R_1 (obs. refl.)	0.0299	0.0322
wR_2 (all data)	0.0777	0.0860
GOF on F^2	0.964	1.054
$\Delta\rho_{max}/\Delta\rho_{min}$ (e Å^{-3})	0.549/−0.509	0.471/−0.331

we had to exclude unresolved solvent by means of SQUEEZE procedure.[42] It is most likely that the sum of the occupation values of the disordered C_2H_5OH molecule is equal to 1. Thus, we add one molecule of ethanol to brutto and moiety formulas. All calculations were performed with the SHELXTL software package.[43] Crystal data and structure refinement parameters are listed in Table 6.

DPPH radical scavenging activity

The free radical scavenging activity was evaluated using the stable radical DPPH, according to the method described by Brand-Williams *et al.* with a slight modification.[44] For each compound a 1 : 1 ratio expressed as moles of compound per mole of DPPH radical was tested. A 1 mL sample of the compound solution in methanol was added to 1 mL of DPPH solution in methanol so that the initial DPPH concentration in the cuvettes was 0.1 mM. The samples were incubated for 30 min at 20 °C in methanol and the decrease in the absorbance values of the DPPH solution were measured at λ_{max} 517 nm on the Zenyth 200RT Anthos microplate spectrophotometer. Results were expressed as scavenging activity calculated as follows:

$$\text{Scavenging activity}, \% = [(A_0 - A_1)/A_0] \times 100$$

The concentration of compound needed to decrease 50% of the initial substrate concentration (EC_{50}) is a parameter widely used to measure the antioxidant effect.[33] For determination of the EC_{50} the values of DPPH decrease after 30 min were used. The EC_{50} values were calculated graphically by plotting scavenging activity against compound concentration. Different sample concentrations (0.01, 0.02, 0.05 and 0.1 mM) were used in order to obtain kinetic curves and to calculate the EC_{50} values.

Linoleic acid peroxidation

The effect of compounds on the linoleic acid peroxidation was estimated according to a known procedure.[45] Phosphate buffer (2 mL, pH 7.4) was added to a solution of linoleic acid (0.034 mL) in ethanol (1.97 mL). The reaction mixture contained a solution of linoleic acid (0.33 mL), a solution of $FeCl_2$ (0.066 mL, 4 mM), phosphate buffer (0.164 mL), and a solution of the compound under study in ethanol (1 mL, 30 mM). The resulting solution was incubated for 30 min at 37 °C, then a solution (0.84 mL) containing 0.25 M HCl, 10% trichloroacetic acid and 0.6% thiobarbituric acid was added. The mixture was heated at 95 °C for 15 min, centrifuged and the absorption at λ_{max} 532 nm was measured on a 96 well plate spectrophotometer.

Lipoxygenase activity

Lipoxygenase (LOX) type 1-B from Glycine max (soybean), boric acid, linoleic acid, ammonium acetate, copper(II) chloride, ethanol (96%) and Trolox were purchased from Sigma-Aldrich and were used with no further purification.

LOX inhibition activity was determined spectrophotometrically by measuring the increase in absorbance at 234 nm for the oxidation of linoleic acid.[46] The reaction mixture contained the test compounds dissolved in 10 μL of DMSO at initial concentrations of 1.5–30 mM (final concentrations 5, 10, 20, 30, 50, 100 μM) or the 10 μL of DMSO (blank) and 2 mL of 0.3 mM linoleic acid in borate buffer (pH = 9.0) and 0.89 mL of borate buffer. The total sample volume was 3 mL, the final concentration of DMSO was 0.33% v/v. The reaction was started by adding 100 μL of lipoxygenase solution (500 units) in borate buffer. The increase in absorbance was recorded every 1 s during 10 min under controlled temperature 25 °C.

The degree of LOX activity (A%) in the presence of the complexes was calculated according to the following.[47]

A, % = (ν_0 in the presence of inhibitor/ν_0 in the absence of inhibitor) × 100, where ν_0 is the initial rate.

The value of the initial rate (ν_0, μM min^{-1}) was calculated according to formula:

$$\nu_0 = \Delta C/\Delta t = \Delta A/\Delta t\varepsilon = tg\alpha/\Delta t\varepsilon$$

where C is the product concentration (hydroperoxy-linoleic acid), t is the reaction time, ε is molar absorbance coefficient of hydroperoxy-linoleic acid, $tg\alpha$ is the slope of the kinetic curve plotted as absorbance *vs.* time.

IC_{50} values were obtained graphically by plotting a logistic curve in coordinates inhibition activity (A, %) *vs.* inhibitor concentration ([I], μM). The general curve equation is the following:

$$A, \% = 100 \times (1/(1 + [I]/IC_{50}))$$

CUPRAC assay (Cu^{2+} reducing)

Neocuproine (2,9-dimethyl-1,10-phenanthroline) was supplied from Sigma Chemical Co. The method proposed by Apak *et al.* was used with slight modification.[34] For this reason 0.05 mL of $CuCl_2$ solution (0.01 M), 0.05 mL of ethanol neocuproine

solution (7.5 mM) and 0.25 mL of ammonium acetate buffer solution (1 M) were added to a test tube, followed by mixing with different concentrations of tested compounds (10–100 μM). The mixtures were kept at room temperature. Absorbance was measured at 450 nm against a reagent blank 30 min later. The increase of reaction mixture absorbance in comparison with control indicates the reduction capability of the test compound.

Results were presented in Trolox-equivalents. $TEAC_{CUPRAC}$ values were obtained graphically using absorbance data and linear calibration curve plotted as absorbance *vs.* Trolox concentration.

Inhibition of superoxide radical anion formation by xanthine oxidase (NBT assay)

EDTA, xanthine, bovine serum albumin, nitroblue tetrazolium, and xanthine oxidase (0.04 MU) were purchased from Sigma-Aldrich Chemical Co. The superoxide anion was generated enzymatically by the xanthine oxidase system. The reaction mixture consisted of 2.70 mL of 40 mM sodium carbonate buffer containing 0.1 mM EDTA (pH 10.0), 0.06 mL of 10 mM xanthine, 0.03 mL of 0.5% bovine serum albumin, 0.03 mL of 2.5 mM nitroblue tetrazolium and 0.06 mL of the sample solution in DMSO. To the mixture at 25 °C, 0.12 mL of xanthine oxidase (0.04 units) was added, and the absorbance at 560 nm (by formation of blue formazan)[48] was recorded by microplate spectrophotometer Zenyth 200rt Anthos for 60 s. A control experiment was carried out by replacing the sample solution with the same amount of DMSO. Inhibition I (%) = $[(1 - A_i/A_0) \times 100\%]$, where A_i is the absorbance in the presence of the testing compound, A_0 is the absorbance of the blank solution. All experiments were performed three times.

Rat brain homogenates preparation

On the day of the experiment adult male rats fasted overnight were euthanized in a CO_2-chamber followed by decapitation. The procedure being in compliance with the Guidelines for Animal Experiments at IPAC RAS. The brain was rapidly removed and homogenized in 0.12 M HEPES saline buffer (HBS) at pH 7.4 (10% w/v), centrifuged at 3000 g at 4 °C for 10 minutes and supernatant was used immediately for assay.

Protein concentrations in rat brain homogenates were determined by the biuret assay using bovine serum albumin as a standard.[49]

Fe^{3+} and ^{t}BHP induced lipid peroxidation assay

The extent of lipid peroxidation was estimated by the levels of malondialdehyde measured using the TBARS assay. Study of compounds influence on lipid peroxidation of the rat brain homogenates were carried out at 30 °C for 40 min in 0.25 mL of the homogenates (2 mg of protein ml^{-1}) in HBS in the presence or absence of compounds or vehicle (DMSO). Lipid peroxidation was induced by using Fe^{3+} (0.5 mM $FeNH_4(SO_4)_2$)[50] or ^{t}BHP as an oxidizing agent. Then, 0.25 mL aliquots were mixed with 0.5 mL of thiobarbituric acid medium containing 250 mM HCl, 15% trichloroacetic acid and 3 mM thiobar, heated at 95 °C for 15 min, cooling at 4 °C. Then probes were centrifuged (10 min at 10 000 *g*) and the supernatants transferred into 96-well plate and absorbance was measured at 530–620 nm at the Wallac Victor 1420 Multilabel Counter (PerkinElmer Wallac). All the experiments were performed using four independent experiments with different brain homogenate preparations. Data are normalized to a control probe with oxidant as 100% and a blank probe with diluent but without oxidizing agent. Preliminary experiments were done and the absence of compounds interaction with thiobarbituric acid was seen. The values are expressed as mean % ± SD. The concentrations of ferrocenes giving half-maximal inhibition (IC_{50}) of lipid peroxidation were determined by dose-effect analysis in Origin 6.1 (Origin Lab Corporation).

Acknowledgements

We greatly thank Prof. Konstantin A. Lyssenko from Nesmeyanov Institute of Organoelement Compounds of RAS for the experimental X-ray structural investigations of complexes and valuable discussions. Also the financial support from Russian Foundation for Basic Research (Grants No 11-03-01165, 11-03-01134, 12-03-00776) is gratefully acknowledged.

References

1 T. W. Hambley, *Dalton Trans.*, 2007, 4929–4937.
2 S. P. Fricker, *Dalton Trans.*, 2007, 4903–4917.
3 M. A. Jakupec, M. Galanski, V. B. Arion, C. G. Hartinger and B. K. Keppler, *Dalton Trans.*, 2008, 183–194.
4 J. Bjernemose, A. Hazell, C. J. McKenzie, M. F. Mahon, L. P. Nielsen, P. R. Raithby, O. Simonsen, H. Toftlund and J. A. Wolny, *Polyhedron*, 2003, **22**, 875–885.
5 J. P. Wikstrom, A. Y. Nazarenko, W. M. Reiff and E. V. Rybak-Akimova, *Inorg. Chim. Acta*, 2007, **360**, 3733–3740.
6 W. A. Chomitz, S. G. Manasian, A. D. Sutton and J. Arnold, *Inorg. Chem.*, 2007, **46**, 7199–7209.
7 B. Kabzinska, *Ann. Pharm. Fr.*, 1964, **22**, 685–687.
8 E. J. O'Neil and B. D. Smith, *Coord. Chem. Rev.*, 2006, **250**, 3068–3080.
9 A. Ojida, S.-K. Park, Y. Mito-oka and I. Hamachia, *Tetrahedron Lett.*, 2002, **43**, 6193–6195.
10 C. Lakshmi, R. G. Hanshaw and B. D. Smith, *Tetrahedron*, 2004, **60**, 11307–11315.
11 C. J. Davies, G. A. Solan and J. Fawcett, *Polyhedron*, 2004, **23**, 3105–3114.
12 E. I. Solomon, T. C. Brunold, M. I. Davis, J. N. Kemsley, S.-K. Lee, N. Lehnert, F. Neese, A. J. Skulan, Y.-S. Yang and J. Zhou, *Chem. Rev.*, 2000, **100**, 235–349.
13 A. Trosch and H. Vahrenkamp, *Inorg. Chem.*, 2001, **40**, 2305–2311.
14 Y. Shimazaki, R. Kabe, S. Huth, F. Tani, Y. Naruta and O. Yamauchi, *Inorg. Chem.*, 2007, **46**, 6083–6090.

15 Q.-Y. Chen, J. Huang, W.-J. Guo and J. Gao, *Spectrochim. Acta, Part A*, 2009, **72**, 648–653.

16 U.S. Patent, US 6127356 A3 03.10.00. J. D. CrapoI. Fridovich, T. Ouru, B. J. Day, J. Brian, R. J. Folz, B. A. Freeman, M. P. Trova and I. Batinik-Haberle, Appl. US 1996-663028, 07.06.96. 97 pp.

17 E. R. Milaeva, D. Shpakovsky, Yu. Gracheva, O. Gerasimova, V. Tyurin and V. Petrosyan, *J. Porphyrins Phthalocyanines*, 2003, **8**, 701–706.

18 E. R. Milaeva, V. Yu. Tyurin, D. B. Shpakovsky, O. A. Gerasimova, Z. Jingwei and Yu. A. Gracheva, *Heteroat. Chem.*, 2006, **17**, 475–480.

19 E. R. Milaeva, S. I. Filimonova, N. N. Meleshonkova, L. G. Dubova, E. F. Shevtsova, S. O. Bachurin and N. S. Zefirov, *Bioinorg. Chem. Appl.*, 2010, Article ID 165482, 6 p.

20 E. R. Milaeva, O. A. Gerasimova, Z. Jingwei, D. B. Shpakovsky, S. A. Syrbu, A. S. Semeykin, O. I. Koifman, E. G. Kireeva, E. F. Shevtsova, S. O. Bachurin and N. S. Zefirov, *J. Inorg. Biochem.*, 2008, **102**, 1348–1358.

21 V. Yu. Tyurin, J. Zhang, A. Glukhova and E. R. Milaeva, *Macroheterocycles*, 2011, **4**, 211–212.

22 E. Milaeva, *Curr. Top. Med. Chem.*, 2011, **11**, 2703–2713.

23 R. R. Grinstead, *Pat. Fr. Demande* 2,462,182 (Cl.B01D11/04).

24 E. R. Milaeva, N. N. Meleshonkova, D. B. Shpakovsky, K. V. Uspensky, A. V. Dolganov, T. V. Magdesieva, A. V. Fionov, A. A. Sidorov, G. G. Aleksandrov and I. L. Eremenko, *Inorg. Chim. Acta*, 2010, **363**, 1455–1461.

25 T. Nagataki, K. Ishii, Y. Tachi and S. Itoh, *Dalton Trans.*, 2007, 1120–1128.

26 Z. He, D. C. Craig and S. B. Colbran, *J. Chem. Soc., Dalton Trans.*, 2002, 4224–4235.

27 A. B. P. Lever and E. I. Solomon, in *Ligand-Field Theory and the Properties of Transition Metal Complexes*, ed. A. B. P. Lever and E. I. Solomon, J. Wiley and Sons, 1999, vol. 1, pp. 1–92.

28 J. Becconsall, S. Clough and G. Scott, *Trans. Faraday Soc.*, 1960, **56**, 459–472.

29 C. R. H. I. de Jonge, H. M. van Dort and L. Vollbracht, *Tetrahedron Lett.*, 1970, **11**, 1881–1884.

30 E. R. Milaeva, *Russ. Chem. Bull.*, 2001, **50**, 573–586.

31 N. N. Meleshonkova, D. B. Shpakovsky, A. V. Fionov, A. V. Dolganov, T. V. Magdesieva and E. R. Milaeva, *J. Organomet. Chem.*, 2007, **692**, 5339–5344.

32 P. Molyneux, *Songklanakarin J. Sci. Technol.*, 2004, **26**, 211–219.

33 J. Ancerewicz, E. Migliavacca, P.-A. Carrupt, B. Testa, F. Brée, R. Zini, J.-P. Tillement, S. Labidalle, D. Guyot, A.-M. Chauvet-Monges, A. Crevat and A. Le Ridant, *Free Radical Biol. Med.*, 1998, **25**, 113–120.

34 R. Apak, K. Guglu, M. Ozyurek and S. Karademir, *J. Agric. Food Chem.*, 2004, **52**, 7970–7981.

35 E. Novo and M. Parola, *Fibrog. Tissue Repair*, 2008, 1, 5. 58pp.

36 D. Salvemini, E. Mazzon, L. Dugo, D. P. Riley, J. L. Zweier, C. Thiemermann, Z. Wang and D. Salvemini, *Br. J. Pharmacol.*, 2001, **132**, 815–827.

37 D. Salvemini, D. P. Riley and S. Cuzzocrea, *Nat. Rev. Drug Discovery*, 2002, **1**, 367–374.

38 J. B. Day and M. Patel, *Drugs Future*, 2008, **33**, 1025–1031.

39 I. Kubo, N. Masuoka, T. J. Ha and K. Tsujimoto, *Food Chem.*, 2006, **99**, 555–562.

40 J. L. Pierre and M. Fontecave, *BioMetals*, 1999, **12**, 195–199.

41 E.-J. Shin, K. Ho Ko, W.-K. Kim, J. S. Chae, T. P. H. Yen, H. J. Kim, M.-B. Wie and H.-C. Kim, *Neurochem. Int.*, 2008, **52**, 1134–1147.

42 A. L. Spek, PLATON software, *J. Appl. Crystallogr.*, 2003, **36**, 7–13.

43 G. M. Sheldrick, *Acta Crystallogr., Sect. A: Fundam. Crystallogr.*, 2008, **64**, 112–122.

44 W. Brand-Williams, M. E. Cuvelier and C. Berset, *Food Sci. Technol.*, 1995, **28**, 25–30.

45 J. K. Callaway, P. M. Beart and B. Jarrott, *J. Pharmacol. Toxicol. Methods*, 1998, **39**, 155–162.

46 I. Ozturk, S. Filimonova, S. K. Hadjikakou, N. Kourkoumelis, V. Dokorou, M. J. Manos, A. J. Tasiopoulos, M. M. Barsan, I. S. Butler, E. R. Milaeva, J. Balzarini and N. Hadjiliadis, *Inorg. Chem.*, 2010, **49**, 488–501.

47 M. N. Xanthopoulou, S. K. Hadjikakou, N. Hadjiliadis, E. R. Milaeva, J. A. Gracheva, V. Yu. Tyurin, N. Kourkoumelis, K. C. Christoforidis, A. K. Metsios, S. Karkabounas and K. Charalabopoulos, *Eur. J. Med. Chem.*, 2008, **43**, 327–335.

48 S. Toda, M. Kumura and M. Ohnishi, *Planta Med.*, 1991, **57**, 8–10.

49 A. G. Gornall, C. J. Bardawill and M. M. David, *J. Biol. Chem.*, 1949, **177**, 751–766.

50 J. K. Callaway, P. M. Beart and B. Jarrott, *J. Pharmacol. Toxicol. Methods*, 1998, **39**, 155–162.

